Evan Copland

Case Western Reserve University / NASA Glenn Research Centre, Department of Materials Science and Engineering, Cleveland, Ohio, USA

Comparing the thermodynamic behaviour of Al(l) + ZrO_2(s) to Al(l) + Al_2O_3(s)

In an effort to better determine the thermodynamic properties of Al(g) and Al_2O(g) the vapour in equilibrium with Al(l)+ZrO_2(s) was compared to the vapour in equilibrium with Al(l)+Al_2O_3(s) over the temperature range 1197-to-1509K. This comparison was made directly by Knudsen effusion-cell mass spectrometry with an instrument configured for a multiple effusion-cell vapour source (*multi-cell KEMS*). Second-law enthalpies of vaporization of Al(g) and Al_2O(g) together with activity measurements show that Al(l)+ZrO_2(s) is thermodynamically equivalent to Al(l)+Al_2O_3(s), indicating Al(l) remained pure and Al_2O_3(s) was present in the ZrO_2-cell. Subsequent observation of the Al(l)/ZrO_2 and vapor/ZrO_2 interfaces revealed a thin Al_2O_3-layer had formed, separating the ZrO_2-cell from Al(l) and Al(g)+Al_2O(g), effectively transforming it into an Al_2O_3 effusion-cell. This behaviour agrees with recent observations made for β-NiAl(Pt) alloys measured in ZrO_2 effusion-cell.

Keywords: KEMS; thermodynamic property measurements; Al(g), Al_2O(g); Al-Zr-O system

1. Introduction

The Al-O system is important to the field of high-temperature oxidation as many Ni-, Ti- and Fe-base alloys rely on a thermally grown Al_2O_3-layer for protection in oxygen containing atmospheres above 1273K. To better understand the formation and growth of Al_2O_3 in contact with an alloy, the thermodynamic activities of Al, O and Al_2O_3 at the alloy/Al_2O_3 interface are needed as a function of alloy composition and temperature [1]. These activities can be measured by comparing the partial pressure of characteristic species in equilibrium with an alloy+Al_2O_3 sample to that in equilibrium with a reference state. These measurements can be made directly with a multiple Knudsen effusion-cell vapour source attached to a mass spectrometer (*multi-cell KEMS*) [1-8]. The usefulness of measured activities ultimately depends on the definition of the experimental reference state and how accurately its thermodynamic properties are known. For Al activity measurements the stability of Al_2O_3 means that the oxide and oxygen vapour pressure must be considered. Therefore the two phase mixture, Al(l)+α-Al_2O_3(s) at the dissociation pressure of O(g), was proposed as an experimental reference for Al, Al_2O, O, and Al_2O_3 [1-3].

The condensed portion of the Al-O system is understood and consists of: two immiscible liquids Al(l) and Al_2O_3(l), the fcc solid solution Al(s), and hexagonal aluminium oxide α-Al_2O_3(s) [9]. The solubility of oxygen in fcc and liquid aluminium is typically below measurement sensitivity (and less then ~0.1 at% at 2323K) and similarly deviations of Al_2O_3 from stoichiometry are not measurable. Therefore at temperatures below 1600K (where the vapour pressure of Al(g) and Al_2O(g) are less then 10^{-4} atm.) both Al(l) and α-Al_2O_3(s) can be considered to be pure substances. The thermodynamic properties of the condensed phases are accurately known as indicated by the reported enthalpy of formation of alumina: $\Delta_f H^o$(α-Al_2O_3(s), 298.15K) = -1675.7 ± 1.3 kJmol^{-1} [10-12]. The vapour phase, however, is more complicated with a range of identified vapour species: Al, Al_2O, Al_2, AlO, AlO_2, Al_2O_2,

Al_2O_3, O and O_2. The vapour composition depends on oxygen partial pressure [13-15]. At low $p(O_2)$ when Al(s,l) and α-Al_2O_3(s,l) are stable and Al(g) and Al_2O(g) dominate while at higher $p(O_2)$ only α-Al_2O_3(s,l) is stable and O(g), Al(g) and AlO(g) are expected to dominate. The thermodynamic properties of these vapour species are not accurately known as shown in Tab. 1.

Table 1. Enthalpy of Formation, $\Delta_f H°(298.15K)$

Species	IVTAN [10] ($kJmol^{-1}$)	JANAF [12] ($kJmol^{-1}$)
Al(g)	330.0±3.0	329.7±4.2
Al_2O(g)	-148.6±22	-145.2±17
Al_2(g)	501.3±20	487.0±3.5
AlO(g)	67.3±6.4	66.9±8.0
AlO_2(g)	-38.8±30	-86.2±32

This uncertainty has a significant effect on the accuracy of Al, O and Al_2O_3 activities measured in a range of important alloy systems. To improve these measurements the thermodynamic properties of the vapour phase in the Al-O system needs further investigation.

The reason for the poor quality of these data is unclear but the choice of container material is always important in thermodynamic measurements and a range of materials (*i.e.*, BeO, TaC, ZrO_2 and Al_2O_3) have been considered in studies of the Al-O system. To determine if the container material has a significant effect on the measured thermodynamic properties of Al(g) and Al_2O(g) this study directly compared the vapour in equilibrium with Al(l)+ZrO_2(s) to that in equilibrium with Al(l)+Al_2O_3(s). The 'second-law' reaction enthalpies involving Al(g) and Al_2O(g) are considered for both mixtures. In addition, the activities of Al, Al_2O, O and Al_2O_3 were determined directly by treating Al(l)+ZrO_2(s) as an alloy and Al(l)+Al_2O_3(s) as the experimental reference state. The Al(l)/ZrO_2 and vapor/ZrO_2 interfaces were investigated after the pressure measurements to provided direct information about the nature of the Al(l)+ZrO_2(s) system and the Al_2O_3(s) + ZrO_2(s) equilibrium [16,17]

at low $p(O_2)$. This study also provides important information supporting the apparent observation of an equilibrated Al_2O_3-layer on the surface of β-NiAl(Pt) alloys during Ni and Al activity measurements made in ZrO_2 effusion-cells [3].

2. Experimental

2.1 Materials

The effusion cells used in this study were machined from dense polycrystalline Al_2O_3-rod (99.9 wt% purity) and partially stabilized zirconia (ZrO_2 ~5.0 wt%Y_2O_3, 99.9 wt% purity). The cells were cleaned prior to this experiment by baking at ~1800K for 10 hours under vacuum (~10^{-8} bar). About 0.5 g of clean Al-shot (99.9999 wt% purity) was loaded into both the ZrO_2 and Al_2O_3 effusion-cell. In addition to the Al samples, pure-Au (99.9999 wt% purity) was placed in an open graphite-cup inside a second Al_2O_3 effusion-cell for use as a temperature and vapour pressure standard.

2.2 Activity measurements

The measurements were made with a Nuclide/MAAS/PATCO 12-90-HT single focus 90° permanent sector mass spectrometer with an electron-multiplier detector. The mass spectrometer was configured for use with a multiple effusion-cell vapour source. A detailed description of the instrument and measurement procedures is found in references 1 and 2. Knudsen effusion-cell mass spectrometry allows the simultaneous determination of the identity and relative pressure of the vapour species in equilibrium with a condensed sample as a function of temperature [4]. The partial pressure of a species, A, is determined indirectly by sampling its flux in a molecular beam (selected from the distribution of effusing molecules) by electron bombardment, the formation of ion, K^+, the subsequent formation of a representative ion beam that is sorted according to mass-to-charge ratio by common mass

spectrometric techniques. The partial pressure, p(A), in the effusion-cell is related to the measured intensity of ion K^+, I_{AK}, and absolute temperature, T, by:

$$p(A) = \frac{I_{AK} T}{S_{AK}} \tag{1}$$

Where, S_{AK} is the instrument sensitivity factor and is a complex function of the: intersection of the molecular and electron beams, ion extraction efficiency, ionisation cross-section, transmission probability of the mass analyser, detection coefficient and isotopic abundance.

The *multi-cell KEMS* configuration involves placing two or more effusion cells in the isothermal zone of a furnace and allows the direct comparison of the partial pressure of a characteristic vapour species in equilibrium with an alloy ($p(A)$, I_{AK}) in one cell to an experimental reference state ($p^o(A)$, I^o_{AK}) in an adjacent cell at one temperature [2,5-8]. As relative partial pressures are considered there is no need to determine an absolute value for S_{AK} and thermodynamic activities can be measured directly according to:

$$a(A) = \frac{p(A)}{p^o(A)} = \frac{I_{AK} \cdot T}{I^o_{AK} \cdot T} \cdot \frac{S^o_{AK}}{S_{AK}} = \frac{I_{AK}}{I^o_{AK}} \cdot \frac{g(ref)}{g(alloy)} \tag{2}$$

All factors in S_{AK} related to ionisation and mass spectra analyses cancel, however, the geometric relation between the molecular- and electron-beam remain which is represented in Eq. (2) by, $g(ref)$ / $g(alloy)$, the 'geometry factor ratio' (*GFR*). Provided the cells are isothermal and molecular beam sampling is independent of the vapour source, the *GFR* for a pair of cells only depends on differences in orifice/cell shape [2,6]. The *GFR* was determined for the Al_2O_3 and ZrO_2 effusion-cell used in this study by comparing the intensity of $^{197}Au^+$ from each cell in a complementary experiment with pure-Au in both cells. A

$g(Al_2O_3)/g(ZrO_2)$ of 0.95±0.01 was determined and was used in Eq. (2) to correct for the variation in effusion-cell and orifice shape between the cells. Fig. 1 shows a schematic of the effusion cells used in this study.

Consistent vapour pressure sampling is obtained with the inclusion of two fixed apertures (field ϕ 1mm and source ϕ 2mm) between the effusion cell and ion source [7,8] and accurate alignment of the effusion-cell orifice [2]. The fixed apertures define an ionisation volume that is independent of vapour source. The alignment of all effusion orifices were visually monitored with a video camera mounted above the ion source chamber that sights through the fixed apertures [2]. The steady state condition in each effusion-cell was verified at each temperature with repeated measurements 30-45 minutes apart. The typical variation in temperature and ion-intensity between repeat measurements was less then 0.5K and 1%, respectively. Measurements were made at a range of temperatures over three days and were taken in a predetermined "random" order to remove systematic errors. Temperature was measured with a pyrometer (*Mikron* M190V-TS) sighting a blackbody source (ϕ 2.5mm x 13.5mm) machined into the bottom of the effusion-cell and Mo-cell holder. The pyrometer was calibrated during the experiment by measuring the melting point of Au (1337.5K) and confirmed with the measured enthalpy of sublimation of Au.

2.3 The Al(l)+α-Al_2O_3 experimental reference state

As Al(l) and α-Al_2O_3(s) remain pure, the Al(l)+α-Al_2O_3(s) experimental reference state defines the equilibrium vapour pressures of Al(g), Al_2O(g) and O(g) according the Eq.(3-5).

$$Al(s,l) = Al(g) \qquad K_1 = p^{\circ}(Al) \tag{3}$$

$$4/3\,Al(s,l) + 1/3\,Al_2O_3(s) = Al_2O(g) \qquad K_2 = p^{\circ}(Al_2O) \tag{4}$$

$$2Al(s,l) + 3O(g) = Al_2O_3(s) \qquad K_3 = 1/p^{*}(O)^3 \tag{5}$$

Where $p^*(O)$ is the vapour pressure of O(g) in equilibrium with the Al(l)+α-Al_2O_3(s) and commonly referred to as the *dissociation pressure* of the oxide. Atomic oxygen is considered because it is the dominant oxygen vapour species (*i.e.*, $p(O) >> p(O_2)$) and it is the species expected to dissolve in an alloy. For alloys with a significant aluminium concentration in equilibrium with an oxide-compound, Al(g) and Al_2O(g) dominant the vapour, allowing $a(Al)$ and $a(Al_2O)$ can be measured directly according to Eq.(2) by: $a(Al) = p(Al)/p^\circ(Al)$ and $a(Al_2O) = p(Al_2O)/p^\circ(Al_2O)$. The quantities $a^*(O)$ and $a(Al_2O_3)$ are determined indirectly from the measured values of $a(Al)$ and $a(Al_2O)$ according to the additional independent reactions in the Al-O system.

$$2Al(g) + O(g) = Al_2O(g) \qquad a^*(O) = \frac{a(Al_2O)}{a(Al)^2} \qquad (6)$$

$$4Al(g) + Al_2O_3(s) = 3Al_2O(g) \qquad a(Al_2O_3) = \frac{a(Al_2O)^3}{a(Al)^4} \qquad (7)$$

Where $a^*(O)$ is an experimental oxygen activity relative to the dissociation pressure of O(g) in equilibrium with Al(l)+α-Al_2O_3(s); in terms of Eq.(2): $a^*(O) = p(O)/p^*(O)$. While different from the traditional reference state, Al(l)+α-Al_2O_3(s) has two important advantages: 1) it has a reactivity very close to that of the alloy/scale interface being studied which makes $a^*(O)$ measurements very sensitive to alloy composition, and 2) it provides a sample that can be physically placed in an effusion-cell adjacent to the effusion-cell containing the alloy sample. This experimental activity can be converted to more conventional values by changing the reference state of oxygen to an ideal gas, O_2(g), with a partial pressure of 1 bar (*i.e.*, $a(O_2) = a^*(O)^2 \cdot K_3^{-2/3}$) [3].

2.4 Analysis of the Al(l)/ZrO_2 and vapor/ZrO_2 interfaces

To obtain direct evidence of any reaction at the Al(l)/ZrO_2 and vapor/ZrO_2 interfaces the ZrO_2 effusion-cell was sectioned, mounted and polished after the vapour pressure measurements. The interface was observed by optical and electron microscopy. The phases at the interface were identified by their composition, which was measured by electron microprobe analysis (*JEOL 8200*) at 15 kV and 30 nanoamps absorbed current. Prior to microprobe analysis the polished samples were coated with approximately 200 angstroms of evaporated carbon. Pure-Al_2O_3, pure-Zr and pure-Y were used as WDS standards for Al, O, Zr and Y respectively.

3. Results

3.1. Relative partial pressures of Al(g), Al_2O(g), Au(g) and measured T_{mp}(Au)

The relative vapour pressures of Al(g) and Al_2O(g) were sampled from the ZrO_2 and Al_2O_3 effusion-cells together with the vapour pressure of Au(g) in equilibrium with pure-Au in a second Al_2O_3 effusion-cell over the temperature range 1197-to-1509K. The experimental data are shown in Fig. 2, as the natural logarithm of the product of ion-intensity and temperature vs. inverse-temperature. In Fig. 2 data from Al(l)+ZrO_2(s) and Al(l)+Al_2O_3(s) are represented by ○ and Δ, respectively. At each temperature the data consists of two sets of 6 measurements taken about 45min apart. The numbers on the Al(g) curve represent the order that the measurements were taken. The pyrometer was calibrated at the start of the experiment by monitoring the detector-current while the furnace was slowly ramped through the melting point of Au [2]. The measured detector-current at the melting point of Au was used to determining the combined emissivity of the black-body source and optic-path (an emissivity of 0.962 was determined and was consistent with previous values). The melting point of Au was also measured at the end of the experiment together with the ion intensity of $^{197}Au^+$ and these values are shown in Tab. 2.

Table 2. Measured Melting Point of Au (1337.58 K)

T_{meas} (K)	Detector Current (nA)	$^{197}Au^{+}$ (cps)
1337.5±0.5	0.7348±0.0047	115.7±5.0
1337.9±0.5	0.7379±0.0039	128.9±5.0

The variation in the ion intensity of $^{197}Au^{+}$ (at the melting point) indicates a significant change in instrument sensitivity during the course of the experiment, which in part was due to operator error. For the Au(g) data taken over a time when the instrument sensitivity remained consistent (indicated by the line of best fit on the Au curve in Fig. 2) the measured enthalpy of sublimation at 298.15K, shown in Tab. 3, agrees with the accepted value (367.04±0.9kJmol^{-1}) [18]. A consistent $\Delta_{sub}H°$(Au, 298.15K) together with an accurate melting point of gold typically indicates good instrument operation. For Al(g) and Al_2O(g) in the Al_2O_3 effusion-cell, the 'second law' enthalpies can be interpreted as sublimation from Al(l)+α-Al_2O_3(s) according to reactions 3 and 4 and are also shown in Tab. 3. The first values are determined from all the data shown in Fig. 2, while the bracketed values represent the data where consistent instrument sensitivity was observed.

Table 3. Second-Law Enthalpies of Sublimation $\Delta_{sub}H$(298.15K)

Species	Al_2O_3-Cell (kJmol^{-1})	ZrO_2-Cell (kJmol^{-1})
Au(g)	375.0±4.6 (365.1±4.7)	~
Al(g)	350.9±2.6 (339.0±5.8)	349.9±2.8 (336.5±8.9)
Al_2O(g)	433.1±2.8 (418.2±5.6)	429.8±3.0 (414.2±9.6)

Bracketed values from data taken during a period of consistent instrument sensitivity.

In addition to variations in instrument sensitivity, condensation of Al_2O_3 on the outer edge of the effusion orifice was observed (visually and as a drop in measured ion-intensities)

for both ZrO_2 and Al_2O_3 effusion-cells at 1487 and 1509K. The combination of Al_2O_3-condensation and variable instrument sensitivity at low temperatures make the 'second-law' enthalpies of Al(g) and Al_2O(g) unreliable. The bracketed values, however, are in close agreement with values previously measured by the author [2].

3.2. Measured activities: a(Al), a(Al_2O), a^*(O) and a(Al_2O_3)

While the data shown in Fig. 2 and Tab. 3 has identified problems they suggest almost identical thermodynamic behaviour of Al(g) and Al_2O(g) in Al_2O_3 and ZrO_2 effusion-cells. The *multi-cell KEMS* technique allows the vapour phase in adjacent effusion-cells to be compared directly, independent of changes in instrument sensitivity. The activities of Al, Al_2O, O and Al_2O_3 were determined according to reactions 3-to-7 for Al(l)+ZrO_2 treated as an alloy and Al(l)+Al_2O_3 as the experimental reference state. These results are shown in Figs. 3-to-6.

3.3. Al(l)/ZrO_2 and vapor/ZrO_2 interfaces

The Al(l)/ZrO_2 and vapor/ZrO_2 interfaces were observed after cooling and revealed two single-phase reaction layers, a thin dark-contrast phase over a thicker light-contrast phase as shown in Figs. 7a and 7b, respectively. The dark-contrast layer was in contact with Al(l) and the vapour phase and was identified, by composition, as Al_2O_3 (Tab. 4). The bulk ZrO_2-cell material was two-phase, tetragonal-ZrO_2 + cubic-ZrO_2, in agreement with it being partially stabilized zirconia with the compositions shown in Tab. 4. The composition of the light-contrast reaction layer is identical to the cubic-ZrO_2 (~3.9 at% Y) observed in the bulk of the cell material. The Al_2O_3-layer in contact with the liquid was thicker (~2-to-6μm) then that in contact with the vapour phase (~1-to-2μm). This is probably purely due to kinetic reasons as the number of Al-atoms available to react with oxygen is a lot greater in the liquid then in the

vapour phase. The thickness of the cubic-ZrO_2 reaction layer, however, appeared independent of the Al containing phase.

Table 4. Measured Phase Compositions (at%) by EPMA.

Phases	Al	O	Zr	Y
Al[§]	100.0±0.5	0.5	~	~
Dark-layer	39.6±0.4	60.3±0.4	~	~
Light-layer	~	66.9±0.4	29.2±0.4	3.91±0.034
ZrO_2-grain 1	~	66.8±0.3	31.8±0.3	1.35±0.07
ZrO_2-grain 2	~	66.9±0.4	29.2±0.4	3.91±0.034

§ This is typical behaviour for pure-Al, the O-signal comes from a native oxide layer

4. Discussion

The results shown in Figs. 2–6 and Tab. 3 indicate that the thermodynamic properties of the equilibrium vapour phase and therefore Al(l)+ZrO_2(s) are identical to Al(l)+Al_2O_3(s). This, however, is not possible according the proposed Al-Zr-O phase-diagram shown in Fig. 8 [19]. According to Fig. 8, the Al(l)/ZrO_2(s) interface is unstable and must react by either: 1) reduction of the ZrO_2-cell and the formation of a range of intermetallic compounds like $ZrAl_3$, or 2) oxidation of Al(l) to form a continuous Al_2O_3-layer that separates the Al from the ZrO_2-cell. The measured activities indicate that the second reaction path exists. The fact that a(Al) was not reduced from unity means that Al(l) remained pure, ZrO_2 was not reduced and no intermetallic compounds formed. The measured $a(Al_2O_3)$ indicates Al_2O_3 was present in the ZrO_2-cell. This reaction behaviour was confirmed by direct observation (Fig. 7). The formation of this Al_2O_3-layer effectively transformed the ZrO_2 effusion-cell to an Al_2O_3 effusion-cell, making it thermodynamically identical to the Al(l)+Al_2O_3(s) reference. Based on these results, an ZrO_2 effusion-cell will not effect the measured thermodynamic properties of Al(g) or Al_2O(g).

According to accepted thermodynamic data [10,12] the dissociation pressure of O(g) in equilibrium with Al(l)+Al_2O_3(s) is a little higher then that expected for the Zr(s)+ZrO_2(s)

equilibrium. These results support this, as the presence of Al_2O_3 maintains ZrO_2 under oxidizing conditions. This combined with the limited stochiometric range of Al_2O_3(s) and limited oxygen solubility in Al(l) allows equilibrium to be obtained inside the ZrO_2 effusion-cell. The source of oxygen required to form the Al_2O_3-layer is unclear but ionic transport of oxygen transport through the wall of the ZrO_2 effusion-cell from the surrounding furnace environment could be expected. It is interesting, however, that a three-phase structure (tetragonal-ZrO_2 + cubic-ZrO_2 + Al_2O_3) was not observed on the ZrO_2-side of the Al_2O_3-layer, as expected form the reported phase-equilibria in the Al_2O_3-ZrO_2-Y_2O_3 system [17]. There was no evidence of dissolved Al in either tetragonal-ZrO_2 or cubic-ZrO_2 as suggested in references [16] and [17]. Similarly there was no evidence of dissolved Zr or Y in Al_2O_3 from either activity or microprobe measurements. It should be noted, however, that in making comparisons with published phase-equilibria of the pseudo binary Al_2O_3-ZrO_2 [16] and pseudo ternary Al_2O_3-ZrO_2-Y_2O_3 [17] systems that the current results are determined at significantly reduced oxygen activities (*i.e.*, for the condition when Al_2O_3 is in equilibrium with metallic aluminium). These results suggest oxygen activity has a significant affect on the phase-equilibria in the Al_2O_3-ZrO_2-Y_2O_3 system. Clearly then the Al-Zr-Y-O quaternary is the important system and this system needs more detailed investigation.

In a recent study [3] the effect of Pt additions on the activity of Al and Ni in β-NiAl(Pt) was considered and the activities of Ni, Al, Al_2O, O and Al_2O_3 were determined in a procedure similar to the one discussed here. For a series of measurements made in ZrO_2-cells, a(Ni), a(Al), a^*(O) and $a(Al_2O_3)$ were determined to be about: 0.3, 0.001, 100 and 2, respectively. The measured $a(Al_2O_3)$ suggested Al_2O_3 was present in the ZrO_2 effusion-cell and there was evidence that a thin Al_2O_3-layer was present on the alloy surface. The increased a^*(O) corresponds to the decreased a(Al) but is also consistent with $a(Al_2O_3)$ being greater then unity. An $a(Al_2O_3)$ greater then unity was attributed to the choice of the experimental reference state, Al(l)+Al_2O_3(s), that defines Al_2O_3 under the least reactive

conditions [20]. The environment in equilibrium with the Ni-Al-Pt had a significant a(Ni), reduced a(Al), increased a^*(O) and a(Pt) compared to the experimental reference state. At remains unclear, however, if this increased reactivity of the Al_2O_3 in equilibrium with β-NiAl(Pt) was due to a structural variation (*e.g.*, δ-Al_2O_3, γ-Al_2O_3 or κ-Al_2O_3) or the introduction of an equilibrium concentration of structural defects in α-Al_2O_3. The current results represent a simplification of the Ni-Al-Pt-Zr-O system considered in [3] to Al-Zr-O. The behaviour of the Al-Zr-O system agrees with the interpretation of the measurements made in the β-NiAl(Pt) + ZrO_2 system. In this case an Al_2O_3-layer was present on the ZrO_2 effusion-cell and the presence of pure-Al, with a(Al) = 1, resulted in the formation of Al_2O_3 that was identical to the experimental reference.

While a ZrO_2 effusion-cell is not a problem, condensation of Al_2O_3 on the outer edge of the effusion-orifice is a difficult problem effecting the measurement of the heats of sublimation of Al(g) and Al_2O(g) in equilibrium with Al(l)+Al_2O_3(s) [2,21,22]. This issue has only received limited attention in the literature but it could be a major reason for the range in thermodynamic properties reported for Al-O vapour species. The effect of Al_2O_3-condensation is more pronounced for small diameter orifices (less then ~1.0mm) and is typically only observable at temperatures above ~1500K. This behaviour is characterized, by the current author, as an identical relative drop in the measured ion-intensities of Al^+ and Al_2O^+ from an effusion-cell over time at constant temperature. This observation shows that Al_2O_3-condensation cannot be due to reduced vaporization coefficients [21,22] but rather most likely results from an increased oxygen activity in the furnace outside the effusion-cell. The issue of Al_2O_3(s)-condensation will be discussed in more detail elsewhere.

5. Conclusions

In an effort to better determine the thermodynamic properties of Al(g) and Al_2O(g) the effect of using a ZrO_2 effusion-cell was considered. A direct comparison was made between the

vapour in equilibrium with Al(l) in a ZrO_2 effusion-cell and Al(l) in a Al_2O_3 effusion-cell. 'Second-law' reaction enthalpies involving Al(g) and Al_2O(g) together with the activities of Al, Al_2O, O and Al_2O_3 were made with a multiple Knudsen effusion-cell configured mass spectrometer (*multi-cell KEMS*) over the temperature range 1197-to-1509K. Unfortunately variations in instrument sensitivity and clogging of the orifice by Al_2O_3-condensation made the 'second-law' enthalpies unreliable. Activity measurements, however, indicate Al(l)+ZrO_2 and Al(l)+Al_2O_3 are thermodynamically equivalent. These measurements showed Al(l) remained pure and Al_2O_3 was present in the ZrO_2-cell. This agreed with the phase-equilibria of the Al-Zr-O system that indicates the Al(l)/ZrO_2 interface is unstable. Observation of the Al(l)/ZrO_2 and vapour/ZrO_2 interfaces revealed that an Al_2O_3-layer had formed on the inner surface of the cell, separating the ZrO_2 from the pure-Al. This effectively transformed the ZrO_2 effusion-cell to Al_2O_3, making it thermodynamically identical to Al(l)+Al_2O_3(s). Oxygen ion transport through the ZrO_2 effusion-cell wall is expected to be the source of oxygen for the formation of Al_2O_3. The Al_2O_3-layer formation observed here supports a similar observation recently made with β-NiAl(Pt) alloys measured in ZrO_2-cells.

6. Acknowledgements

The help of Brian Gleeson, David Young and Christian Chatillon is gratefully acknowledged. The funding for this work came from NASA Glenn Research Center's Low Emission Alternative Power Project. Analysis of the reaction products at the Al(l)/ZrO_2 interfaces was performed by James Smith, at NASA Glenn Research Center.

References:

1. E. Copland, *"Measuring the Thermodynamics of the Alloy/Scale Interface"* to appear in High Temperature Corrosion and Materials Chemistry,V, eds. E. Opila, J.Fergus,T. Maruyama, J. Mizusaki, T. Narita, D. Shifler, E. Wuchina, The Electrochemical Society, Pennington, NJ, 2005.
2. E. Copland, N. Jacobson, *NASA Report,* in preparation…
3. E. Copland, *NASA Report*, NASA/CR-2004-211330, (2004).
4. M. Inghram, J. Drowart: "*Mass Spectrometry Applied to High Temperature Chemistry*" in High Temperature Technology, Oct 6-9, (1959), 338.
5. A. Büchler, J. Stauffer: in Thermodynamics (IAEA Vienna, 1966) vol. 1, 271.
6. C. Chatillon, C. Senillou, M. Allibert, A. Pattoret: *Rev. Sci. Instrum.* **47**(3), (1976) 334.
7. P. Morland, C. Chatillon, P. Rocabois: *High Temp. and Materials Sci.* **37**, (1997) 167.
8. C. Chatillion, L. Malheiros, P. Rocabois, M. Jeymond: *High Temp. High Pressures*, **34**, (2002) 213.
9. H. Wriedt: *Bull. Alloy Phase Diagrams*, 6(6), (1985).
10. L. V. Gurvich, I. V. Veyts, C. B. Alcock: *Thermodynamic Properties of Individual Substances, English Version*, Begell House, (1996).
11. J. Cox, D. Wagman, V. Medvedev: CODATA Key Values for Thermodynamics, Hemisphere Publishing Corp. Washington, (1988).
12. M. W. Chase: *NIST-JANAF Thermochemical Tables, 4th Ed.*, American Chemical Society, (1998).
13. L. Brewer, A. Searcy: *J. Am. Chem. Soc.*, **73**, , (1951) 5308.
14. R. Porter, P Schissel, M. Inghram: *J. Chem. Phys,* **23**(2), (1955) 339.
15. J. Drowart, G. DeMaria, R. Burns, M. Inghram: *J. Chem. Phys,* **32**(5), (1960) 1366.

16. S. Lakiza, L. Lapato: *J. Am. Ceram. Soc.* **80**(4), (1997) 893.

17. O. Fabrichnaya, F. Aldinger: *Z. Metallkd.*, **95**(1), (2004) 27.

18. R. C. Paule, J. Mandel: *Analysis of Interlaboratory Measurements on the Vapor Pressure of Gold*, SRM 745, National Bureau of Standards Special Publication 260-19, (1970). Also published in *Pure and Applied Chem.* **31**, (1972) 371.

19. M. Rother, H. Holleck: *J. Chim. Phys.-Chim. Biol.*, **90**(2), (1993) 333.

20. C. H. P. Lupis, Chemical Thermodynamics of Materials, North-Holland, New-York, (1983).

21. O. Herstad, K. Motzfeldt: *Rev. Hautes Tempér. et Réfract.*, **3**, (1966) 291.

22. D. Bhogeswara, K. Motzfeldt: *Acta Chem. Scand.* **24**(8), (1970) 2796.

Correspondence address:

Evan Copland, Dr.

NASA-Glenn Research Center

21000 Brookpark Rd.

Mail Stop 106-1

Cleveland, Ohio 44135

Tel.: +1 216 433-3738

Fax: +1 216 433-5544

E-Mail: Evan.Copland@grc.nasa.gov

Figure captions

Figure 1. ZrO_2 and Al_2O_3 effusion-cells: internal cell-body dimensions ϕ 10mm x 8.6mm, orifice dimensions ϕ 1.0mm x 3.5mm. The orifice offset by 2mm from cell centerline while the hole in the bottom is part of black-body source (ϕ 2.5mm x 13.5mm) for temperature measurement.

Figure 2. Experimental data: natural logarithm of the measured ion-intensity and temperature vs. inverse-temperature. ($\bigcirc$ – Al(l)+ZrO_2(s), Δ – Al(l)+Al_2O_3(s) and $\diamond$ – pure-Au.)

Figure 3. Measured a(Al) as a function of temperature, Al(l)+ZrO_2 as the alloy and Al(l)+Al_2O_3 as the experimental reference state.

Figure 4. Measured $a(Al_2O)$ as a function of temperature, Al(l)+ZrO_2 as the alloy and Al(l)+Al_2O_3 as the experimental reference state.

Figure 5. Measured of a^*(O) as a function of temperature, Al(l)+ZrO_2 as the alloy and Al(l)+Al_2O_3 as the experimental reference state.

Figure 6. Measured of $a(Al_2O_3)$ as a function of temperature, Al(l)+ZrO_2 as the alloy and Al(l)+Al_2O_3 as the experimental reference state.

Figure 7. a) Al(l) / ZrO_2 interface, secondary electron image, 15kV, 1000x; b) Al(g)+Al_2O(g) / ZrO_2 interface, backscattered image, 15kV, 1000x.

Figure 8. Proposed isothermal-section of the Al-Zr-O phase-diagram from reference [19].

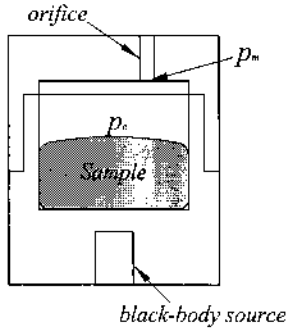

Figure 1. ZrO_2 and Al_2O_3 effusion-cells: internal cell-body dimensions ϕ 10mm x 8.6mm, orifice dimensions ϕ 1.0mm x 3.5mm. The orifice offset by 2mm from cell centerline while the hole in the bottom is part of black-body source (ϕ 2.5mm x 13.5mm) for temperature measurement.

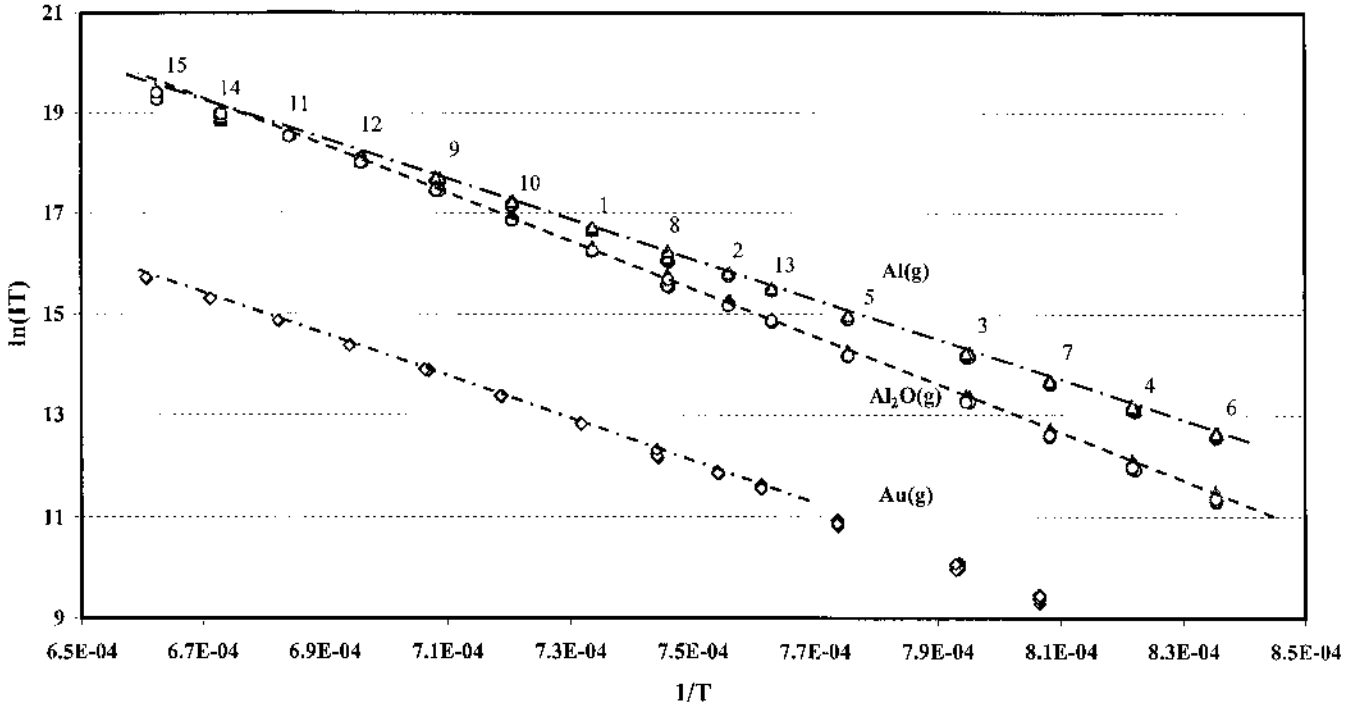

Figure 2. Experimental data: natural logarithm of the measured ion-intensity and temperature vs. inverse-temperature. (○ – Al(l)+ZrO_2(s), Δ – Al(l)+Al_2O_3(s) and ◇ – pure-Au.)

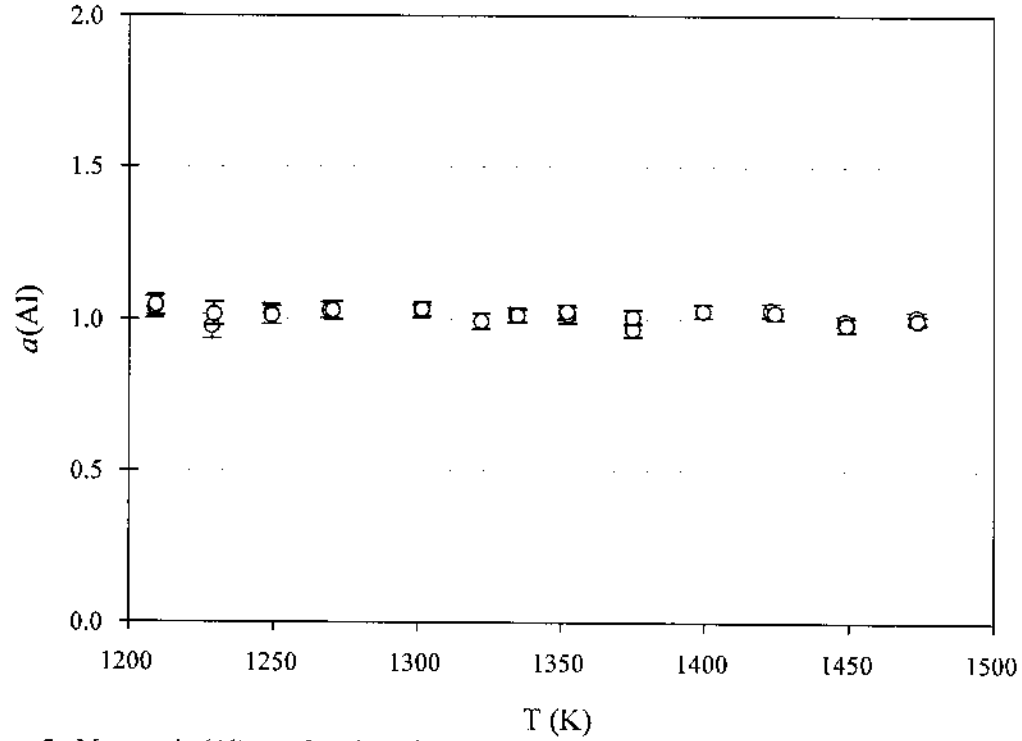

Figure 3. Measured a(Al) as a function of temperature, Al(l)+ZrO_2 as the alloy and Al(l)+Al_2O_3 as the experimental reference state.

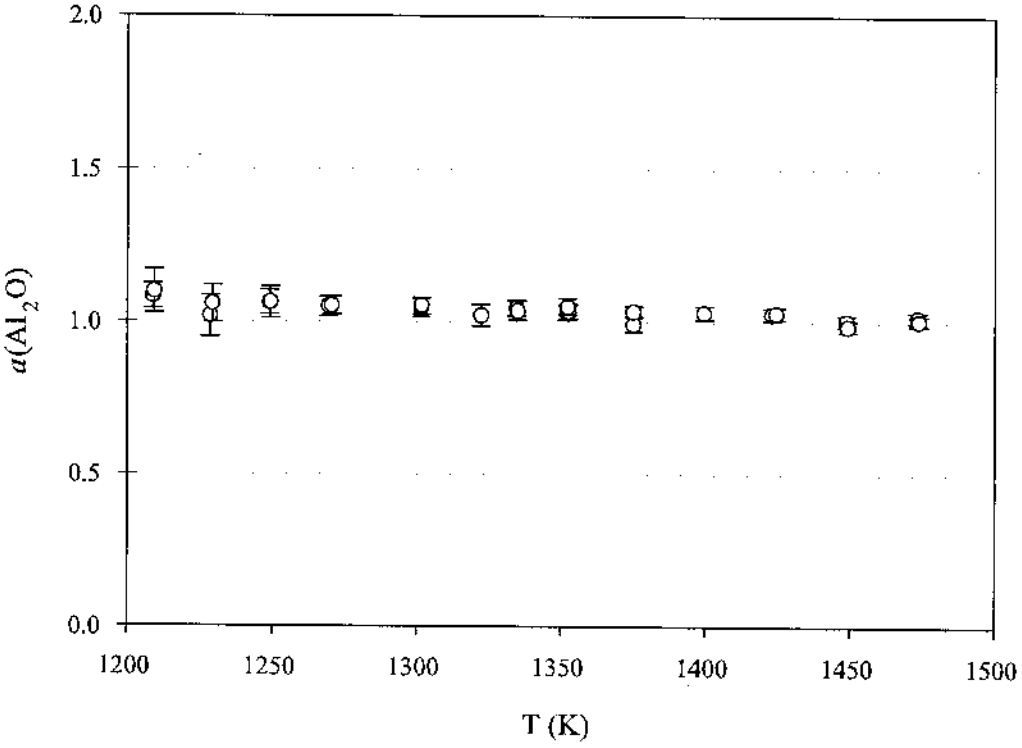

Figure 4. Measured $a(Al_2O)$ as a function of temperature, Al(l)+ZrO_2 as the alloy and Al(l)+Al_2O_3 as the experimental reference state.

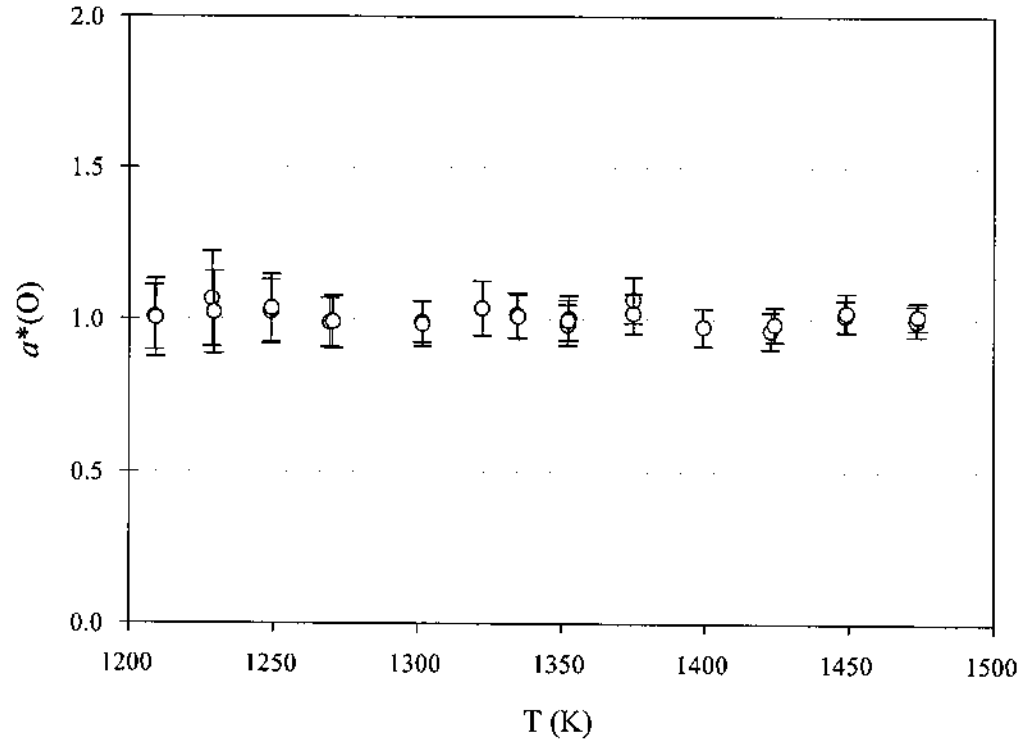

Figure 5. Measured of $a^*(O)$ as a function of temperature, Al(l)+ZrO_2 as the alloy and Al(l)+Al_2O_3 as the experimental reference state.

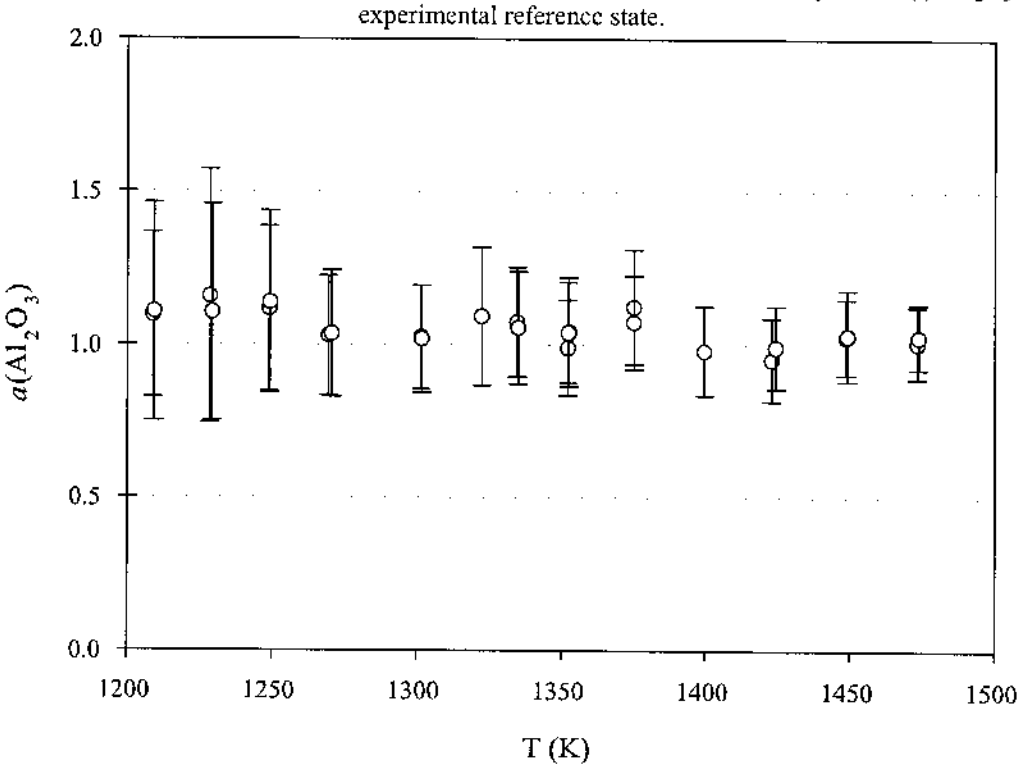

Figure 6. Measured of $a(Al_2O_3)$ as a function of temperature, Al(l)+ZrO_2 as the alloy and Al(l)+Al_2O_3 as the experimental reference state.

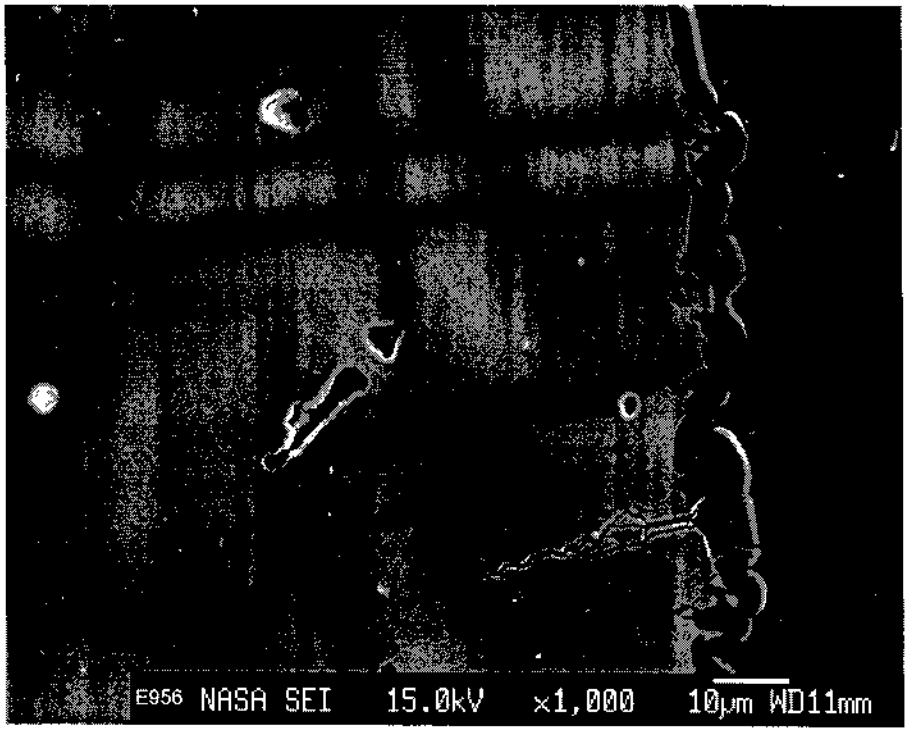

a

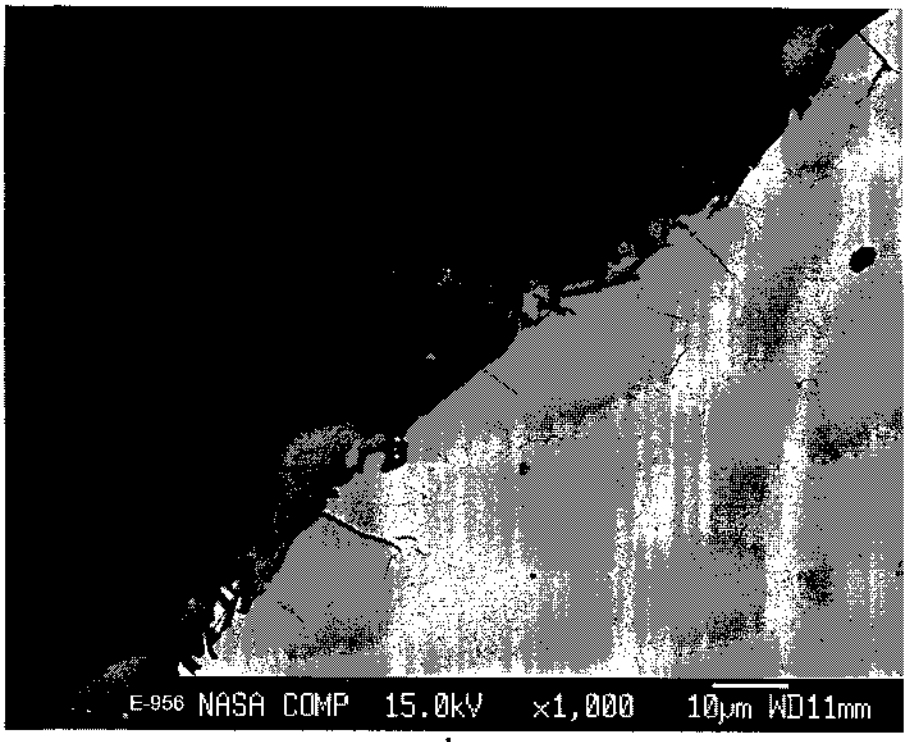

b

Figure 7. a) Al(l) / ZrO_2 interface, secondary electron image, 15kV, 1000x; b) Al(g)+Al_2O(g) / ZrO_2 interface, backscattered image, 15kV, 1000x.

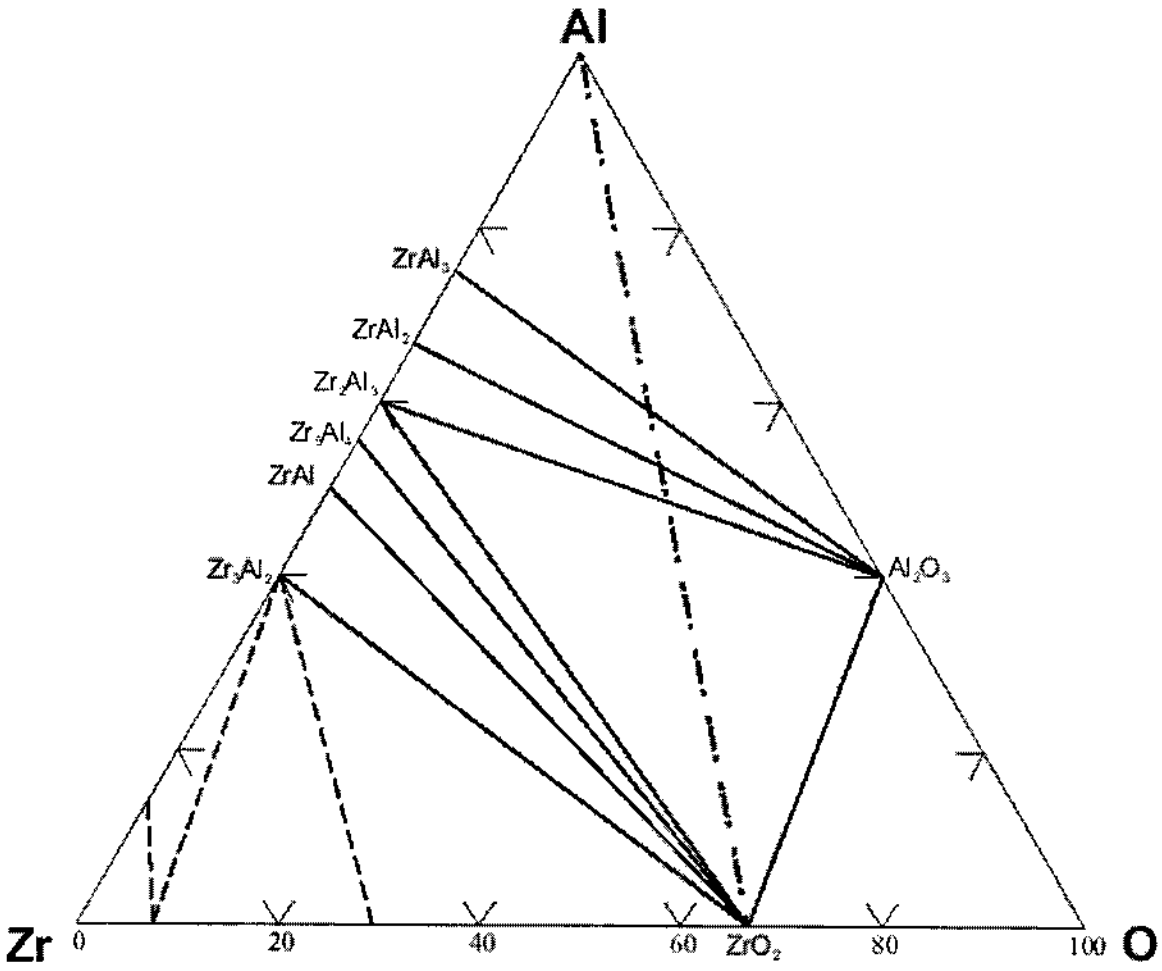

Figure 8. Proposed isothermal-section of the Al-Zr-O phase-diagram from reference [19].